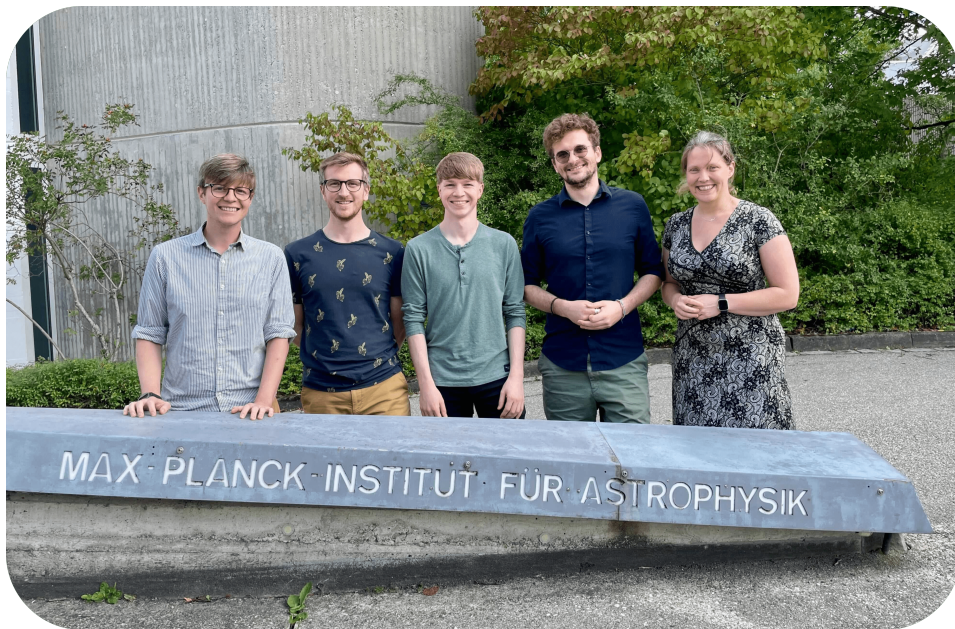


The Asteroseismic Imprints of Mass Transfer

Tom Wagg



Kavli Summer Program Report

September 2023



The Asteroseismic Imprints of Mass Transfer

Kavli Summer Program 2023 Report

TOM WAGG ^{1,2} COLE JOHNSTON ^{3,4} EARL P. BELLINGER ^{2,5} MATHIEU RENZO ⁶ AND SELMA E. DE MINK ²

¹*Department of Astronomy, University of Washington, Seattle, WA, 98195*

²*Max-Planck-Institut für Astrophysik, Karl-Schwarzschild-Straße 1, 85741 Garching, Germany*

³*Department of Astrophysics, IMAPP, Radboud University Nijmegen, PO Box 9010, 6500 GL Nijmegen, The Netherlands*

⁴*Institute of Astronomy, KU Leuven, Celestijnenlaan 200D, 3001 Leuven, Belgium*

⁵*Department of Astronomy, Yale University, CT, 06511, USA*

⁶*Center for Computational Astrophysics, Flatiron Institute, 162 Fifth Ave, New York, NY, 10010, USA*

(Received September 12, 2023)

ABSTRACT

We present new simulations investigating the impact of mass transfer on the asteroseismic signals of slowly pulsating B stars. We use **MESA** to simulate the evolution of a binary star system and **gyre** to compute the asteroseismic properties of the accretor star. We show that, compared to a single star of the same final mass, a star that has undergone accretion has a significantly different internal structure, evident in both the hydrogen abundance profile and Brunt–Väisälä frequency profile. These differences result in significant changes in the observed period spacing patterns, implying that one may use this as a diagnostic to test whether a star’s core has been rejuvenated as a result of accretion. We show that one may draw misleading conclusions of stellar properties when only assuming single star evolution in fitting procedures. Our proof of principle analysis demonstrates the need to further investigate the impact of binary interactions on stellar asteroseismic signals for a wide range of parameters, such as initial mass, amount of mass transferred and the age of the accretor star at the onset of mass transfer.

Keywords: Asteroseismology, Binary stars, Interacting binary stars, Multiple star evolution, Stellar evolution, Roche lobe overflow

1. INTRODUCTION

The majority of massive stars are born in binaries and multiple systems (e.g. Mason et al. 2009; Almeida et al. 2017; Moe & Di Stefano 2017), a large subset of which will exchange mass (e.g. Sana et al. 2012). However, mass transfer, both the process itself and the impact it has on the component stars, is still highly uncertain. This means that there are large uncertainties in evolutionary calculations and predictions, such as the rate of formation of close double compact objects and gravitational wave sources (e.g. Broekgaarden et al. 2022).

There are still many uncertainties in the effect that mass transfer has on mass-gainers, despite the many investigations into understanding the diversity of mass-

losers. Among these uncertainties a key question is whether a mass-gainer will be rejuvenated, where convective cores in accretors grow to account for the additional mass (e.g. Neo et al. 1977), and if so, to what extent. To date, there is no strong observational diagnostic for determining whether the core of a star has been rejuvenated.

Asteroseismology probes the internal structure of stars and so may hold the key to constraining rejuvenation. It is well established that asteroseismology can be used to estimate precise stellar masses, radii and ages based on stellar oscillation modes (Aerts et al. 2010). In particular, main sequence gravity (g) mode pulsators can be observed deep into their radiative envelopes using high-order g -mode oscillations. These pulsators include Slowly Pulsating B (SPB) stars, driven by the κ -mechanism (Waelkens & Rufener 1985; Waelkens 1991; Cox et al. 1992; Pamyatnykh 1999). g -mode pulsators

have been used to provide insights into many aspects of stellar evolution, such as the mass of stellar cores (Johnston 2021; Pedersen 2022) internal mixing processes, and angular momentum transport (Aerts et al. 2019). Recently, g -mode asteroseismology has been used to probe the chemical and temperature gradients outside of the cores of massive stars (Michielsen et al. 2021; Pedersen et al. 2018).

These insights into stellar properties are possible due to the intricate dependence of period spectrum of g -mode pulsations on the size of the convective core and the chemical composition gradient outside of the core (e.g. Miglio et al. 2008). Based on these measured properties, one can infer precise estimates of stellar masses and radii, as well as stellar ages and internal structure properties with additional assumptions of stellar evolution.

Current works only consider single star evolution when inferring stellar properties. However, mass transfer can profoundly influence the structure and composition gradients of accreting stars even after thermal readjustment, as indicated by numerous studies using 1D stellar evolution codes (Renzo & Götzberg 2021; Miszuda et al. 2021). These changes in structure are usually a result of rejuvenation.

As the frequencies of self-excited stellar pulsations are finely tuned by the internal structure of stars, asteroseismology holds the potential to identify the signature of previous mass transfer in various classes of pulsating stars. Furthermore, assuming single star evolution for a star that has undergone accretion may result in misleading inferences of its stellar properties from asteroseismology.

In this paper we assess the impact that mass transfer leaves on the asteroseismic signal of pulsating stars that have recently gained mass through binary interaction. In particular we focus on SPB stars as they are numerous, easily observationally identifiable and have a relatively high binary fraction. We use the 1D stellar evolution code *MESA* to demonstrate the difference in evolution between an accreting star and an equivalent single star. Using the *GYRE* stellar oscillation code we show how these differences in evolution influence the period spacing pattern of an accreting star and highlight how this could affect the inferred properties of the star if single stellar evolution was assumed.

2. BINARY STELLAR EVOLUTION

In this Section we outline the setup of our *MESA* binary models and describe the evolution of the system, both across the Hertzsprung-Russell diagram and in terms its internal structure.

2.1. Model setup

We use Modules for Experiments in Stellar Astrophysics (*MESA*, Paxton et al. 2011, 2013, 2015, 2018, 2019; Jermyn et al. 2023) version r23.05.01 (Paxton 2023) to simulate non-rotating models for a binary system, as well as a grid of single stars against which to compare. Our full inlists are available on GitHub¹ and our model outputs are available on Zenodo².

In particular, the most pertinent settings that we change from the defaults for this work are as follows: We adopt the Ledoux (1947) criterion to account for the presence of a chemical gradient when determining the stability of convection. We include semiconvection following Langer et al. (1983) with a scaled efficiency of $\alpha_{\text{thm}} = 0.1$. For accretors we include thermohaline mixing once they finish accretion following Kippenhahn et al. (1980) with an efficiency of $\alpha_{\text{SC}} = 1$. We use exponential core overshooting from Herwig (2000), setting $(f, f_0) = (0.01, 0.005)$ (Claret & Torres 2017). We set a minimum diffusive mixing coefficient of $20 \text{ cm}^2 \text{ s}^{-1}$; this smooths out any numerical discontinuities in the composition gradients and accounts for a lack of rotational mixing in our models. We motivate our choice of $20 \text{ cm}^2 \text{ s}^{-1}$ and highlight the effect of changing the mixing coefficient on our results in Appendix A. We follow the Kolb & Ritter (1990) prescription to the mass transfer rate with an implicit scheme. We do not account for any rotation in our models. Although we expect that a typical pulsator will likely have some level of rotation, we restrict our proof of principle analysis to less complex non-rotating models. We discuss this choice further in Section 4.2.

Our binary model has a donor with an initial mass of $4 M_{\odot}$ and an accretor with an initial mass of $3 M_{\odot}$, following the typical mass range of SPB stars (Waelkens & Rufener 1985; Waelkens 1991; Kurtz 2022), with an initial period of 5 days and metallicity $Z = 0.02$. We evolve this system up to Roche Lobe overflow and proceed with mass transfer until the secondary accretes $0.5 M_{\odot}$. At this point we end mass transfer, detach the binary and reduce the donor to a point mass, since we are no longer interested in the properties of the donor and thus only track the evolution of the accretor from this point onwards. Although our choice of $0.5 M_{\odot}$ is somewhat arbitrary, this amount could be obtained through different choices of mass transfer efficiencies and the spin-up of the accretor would likely hinder accretion in a similar manner. By constructing our model in this way we are

¹<https://github.com/TomWagg/mass-gainer-seismology>

²<https://zenodo.org/record/>

able to account for a realistic, variable accretion rate. We then evolve the rejuvenated accretor until central hydrogen depletion. Additionally, for comparison, we evolve a grid of single stars with masses from $3\text{--}6 M_{\odot}$ until the end of helium core burning.

2.2. Hertzsprung-Russell diagram evolution

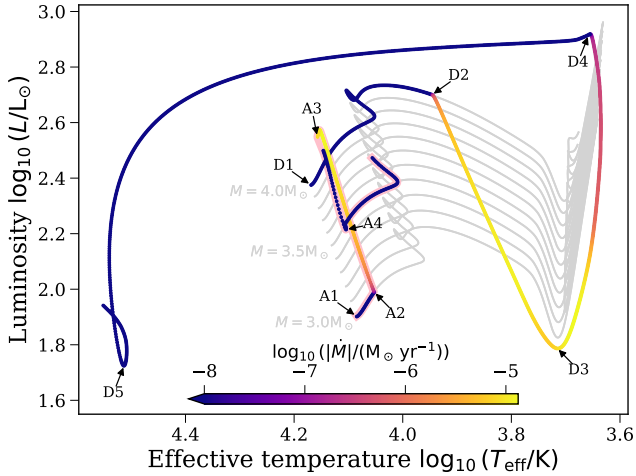


Figure 1. Hertzsprung-Russell diagram showing the evolution of the binary. Tracks are shown for both the donor and accretor, coloured by the absolute mass transfer rate. We highlight the accretor track with a pink outline. Single star tracks added as background grey curves, with masses from 3 to $4 M_{\odot}$ in $0.1 M_{\odot}$ intervals. Important points in the evolution are annotated with arrows and described in the text.

In Figure 1 we show the evolution across the Hertzsprung-Russell diagram of both the donor and accretor of our binary model, with a subset of our single stellar models in the background.

The evolution of the donor (starting at D1) initially follows the $4 M_{\odot}$ single star track, expanding across the main sequence, turning-off and moving across the Hertzsprung gap. Midway through the expansion on the Hertzsprung gap, at point D2, the donor overflows its Roche Lobe and diverges from the single star track, decreasing in luminosity as it transfers mass. As the mass transfer proceeds the orbit of the binary shrinks, increasing the mass transfer rate until the point of closest approach at D3. With the reversal of the mass ratio, mass transfer then causes the orbit to widen, decreasing the mass transfer rate and allowing the donor to increase in luminosity once more. Once the orbit widens to such an extent that Roche lobe overflow ceases (at point D4), the donor relaxes on a thermal timescale, before proceeding with helium core burning from point D5 onwards.

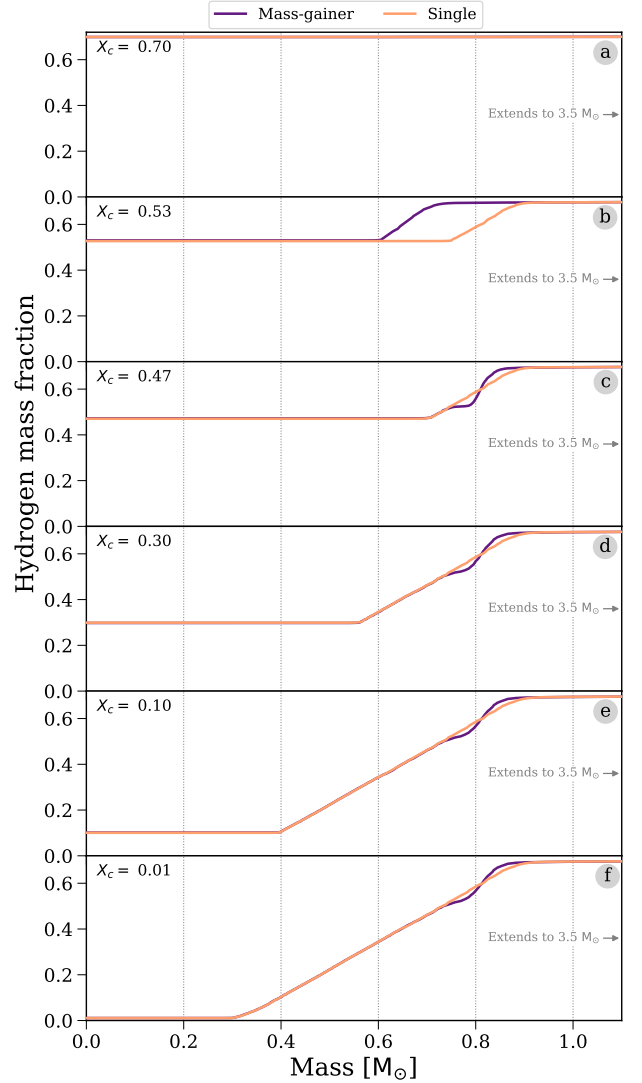


Figure 2. Comparison of the hydrogen abundance profiles between (i) an initially $3 M_{\odot}$ star that accretes mass from a companion and (ii) a single star with the same final mass of $3.5 M_{\odot}$. Each panel compares the stars at the same central hydrogen abundance, which is annotated in each panel.

The evolution of the accretor (highlighted in pink) follows the $3 M_{\odot}$ single star track initially (starting from point A1), but early into its main sequence evolution the donor initiates mass transfer (at point A2) and the accretor increases in luminosity to compensate. Once mass transfer ceases at point A3, the accretor returns to thermal equilibrium at point A4 and proceeds with its main sequence evolution along the $3.5 M_{\odot}$ single star track.

2.3. Rejuvenation and chemical gradients

Although the accretor appears to simply follow a more massive single star track in the Hertzsprung-Russell di-

agram, its *internal* structure has been altered to support the incoming mass, leading to a rejuvenated core (). This is evident in the hydrogen abundance profile of the star, which we plot in Figure 2. In each panel we compare the accretor of our binary model with a $3.5 M_{\odot}$ single star, thus the stars have the same final mass. We highlight that in this figure mass transfer occurs between panels b and c and discuss the difference below.

First, we consider the evolution of the abundance profile for the single star. As the star evolves, it burns hydrogen in its core, decreasing the central hydrogen abundance. At the same time, the reduced hydrogen abundance decreases the opacity of the edge of the core, allowing radiation to travel more freely, leading to a recession of the convective core (Mitalas 1972; Crowe & Matalas 1982; Miglio et al. 2008; Silva Aguirre et al. 2011). As the core recedes it has a decreasing hydrogen abundance, and therefore it imprints a composition gradient in its wake in the abundance profile. We see these trends in Figure 2 as the single star (shown in orange) evolves, with the central abundance decreasing and the imprinted chemical composition gradient extending over time (in the region with diagonal lines).

For the mass-gainer the evolution initially proceeds in a similar manner. In panel b, the shape is similar to that of the single star, though with a smaller convective core due to the star’s initially lower mass. Between panels b and c, mass transfer occurs. As mass transfer proceeds the accretor increases in luminosity to compensate for the additional mass. This leads to an increase in the convective core size, which one can see as the profiles move outwards in mass coordinates in Figure 3. At the same time this core expansion leads to a rejuvenation of the accretor as more hydrogen is mixed into the core, increasing the central abundance (Neo et al. 1977). The expansion of the core into the region through which it previously receded sharpens the composition gradient, resulting in the ‘kink’ in the abundance profile relative to the single star for the remaining panels of Figure 2. The origin of this feature is shown in Figure 3, where we see the hydrogen abundance increase and extend outwards as the core rejuvenates, thus washing away the previous gradient. Returning to Figure 2, the evolution of the abundance profile after mass transfer proceeds similarly to the single star, with subsequent recession of the core and a resulting composition gradient. Critically however, the feature arising from mass transfer remains throughout the main sequence (albeit marginally smoothed by internal mixing).

3. ASTEROSEISMIC SIGNALS

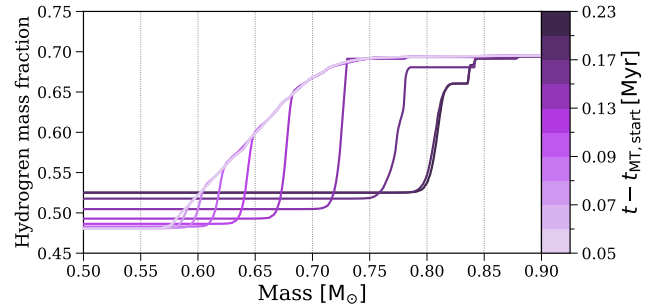


Figure 3. Hydrogen abundance profile of our accretor model during mass transfer. Each line is coloured by its time after the start of mass transfer. This plot shows more time-resolved evolution between panels b and c of Figure 2.

In this Section we demonstrate how the differences in internal structure between the accretor and single star lead to altered asteroseismic signals. We first consider how the Brunt–Väisälä frequency profile is changed, before showing how this influences the period spacing patterns.

3.1. Brunt–Väisälä frequency profile

The Brunt–Väisälä frequency (Väisälä 1925; Brunt 1927), N , defines the regions in which convective instabilities can occur, such that $N^2 < 0$ indicates a convective region, and $N^2 > 0$ a radiative region in which g -modes can propagate³. The Brunt–Väisälä frequency directly determines the period distribution of g -mode oscillations and thus it is pertinent to consider the impact of mass transfer on it. For an ideal gas the frequency can be approximated as

$$N^2 \approx \frac{g^2 \rho}{P} (\nabla_{\text{ad}} - \nabla + \nabla_{\mu}), \quad (1)$$

where ρ is the density, P is the pressure, $\nabla_{\text{ad}} = 2/5$ is the adiabatic temperature gradient and assumed to be a constant, ∇ is the temperature gradient and ∇_{μ} is the chemical composition gradient. We highlight that although many of the terms in this expression are similar for our accretor model and equivalent single star model, the density profile and, as noted in Section 2.3, the composition gradient ∇_{μ} show significant differences and as such we expect similar differences in the Brunt–Väisälä frequency profile.

In Figure 4 we compare, for the same central hydrogen content, the Brunt–Väisälä frequency profiles for the accretor star model and single star model with the same

³The Brunt–Väisälä frequency was originally derived for us in meteorology and only later applied to stellar evolution. We encourage the interested reader to read the original derivation in Brunt (1927)

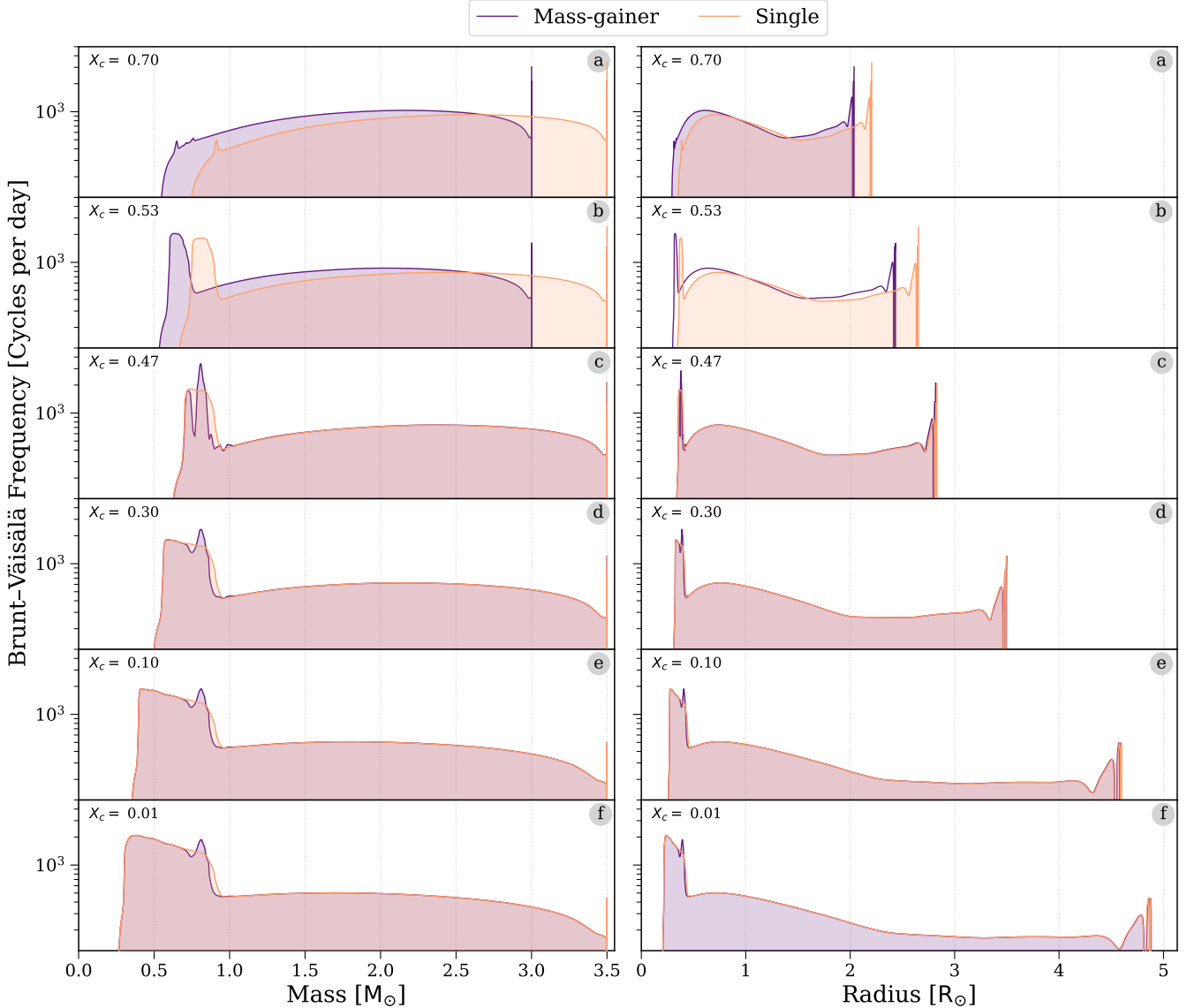


Figure 4. As Figure 2, but showing the Brunt–Väisälä frequency profile for the same evolutionary timesteps. **Left:** as a function of mass coordinate, **right:** as a function of radial coordinate.

final mass. Each panel is for the same central hydrogen content as in Figure 2 for simple comparison. We additionally show the profile as both a function of mass coordinate and radial coordinate in the two columns.

Considering first the single star model, we see that initially the convective core ($N < 0$) extends to $\sim 0.75 M_{\odot}$ (or $\sim 0.3 R_{\odot}$) and the frequency profile changes smoothly across the star. As the star evolves, the core recedes, leaving behind a chemical gradient; a peak then emerges in the Brunt–Väisälä frequency profile that extends between the core and the unmixed outer regions of the star. This peak is directly due to the chemical composition gradient imprinted on the star by the receding core during the main sequence. As the star evolves, the peak

extends in concert with the recession of the core, in line with the composition gradient.

For the accretor model, we see similar evolution in panels a and b (before mass transfer occurs). Immediately following mass transfer (in panel c), the convective core size aligns with the single star model and several sharp features emerge outside of the core, arising due to the kink in the composition gradient visible in panel c of Figure 2. As the star evolves, mixing smooths these features to some extent, but importantly the star retains a double-peaked Brunt–Väisälä frequency profile for the rest of its main sequence evolution.

The Brunt–Väisälä frequency profile of the accretor is inaccessible through single star evolution, which would

always result in a smooth, unimodal peak due to the monotonic change in central hydrogen content.

3.2. Period spacing patterns

All differences between the mass-gainer and equivalent single star that we have noted so far are within the internal structure, and so are not directly observable. Therefore we now consider the impact of these internal structure changes on the observable period spacing pattern.

The period spacing pattern is defined as the difference in period between modes of the same spherical degree, ℓ , and neighbouring radial order, n . Under the assumption of spherical symmetry and high radial order, this difference is constant and follows the asymptotic g -mode period spacing given by [Tassoul \(1980\)](#):

$$\Delta P_g = \frac{\pi^2}{\sqrt{\ell(\ell+1)}} \left[\int_{r_0}^{r_1} \frac{N}{r} dr \right]^{-1}, \quad (2)$$

where ℓ is the spherical degree, N is the Brunt–Väisälä frequency (see Eq. 1) and r_0 and r_1 are the boundaries of the oscillation cavity, which in our model correspond to the convective core boundary and the outer edge of the star respectively.

Deviations from the asymptotic period spacing occur due to abrupt shifts in the Brunt–Väisälä frequency profile, which trap particular modes in certain regions of the star, altering their periods relative to the regular pattern (e.g. [Miglio et al. 2008](#)). The sensitivity of these deviations to the Brunt–Väisälä frequency thus makes the period spacing pattern a useful observable for probing the internal structure of a star.

We use the `GYRE` stellar oscillations code ([Townsend & Teitler 2013](#); [Townsend et al. 2018](#); [Goldstein & Townsend 2020](#); [Sun et al. 2023](#)) to calculate the periods of the $\ell = 1, m = 0$ g -modes for both our accreting star and equivalent single star models. We scan periods from 0.1 to 4 days and solve the full 6th order dimensionless stellar oscillation equations using the Colloc scheme ([Dziembowski 1971](#); [Christensen-Dalsgaard 2008](#)).

In Figure 5 we compare the period spacing pattern of a mass-gainer to that of an equivalent single star at different stages during their evolution. At the zero-age main sequence (in panel a), the period spacing pattern closely follows each star’s asymptotic period spacing (denoted as dotted lines) due to the lack of any composition gradients. Early during the main sequence, immediately prior to mass transfer (in panel b), the pattern now displays some oscillation around the asymptotic value due to the chemical composition gradients that have developed outside of the core. Since this is currently pre-accretion, the stars have different masses and thus con-

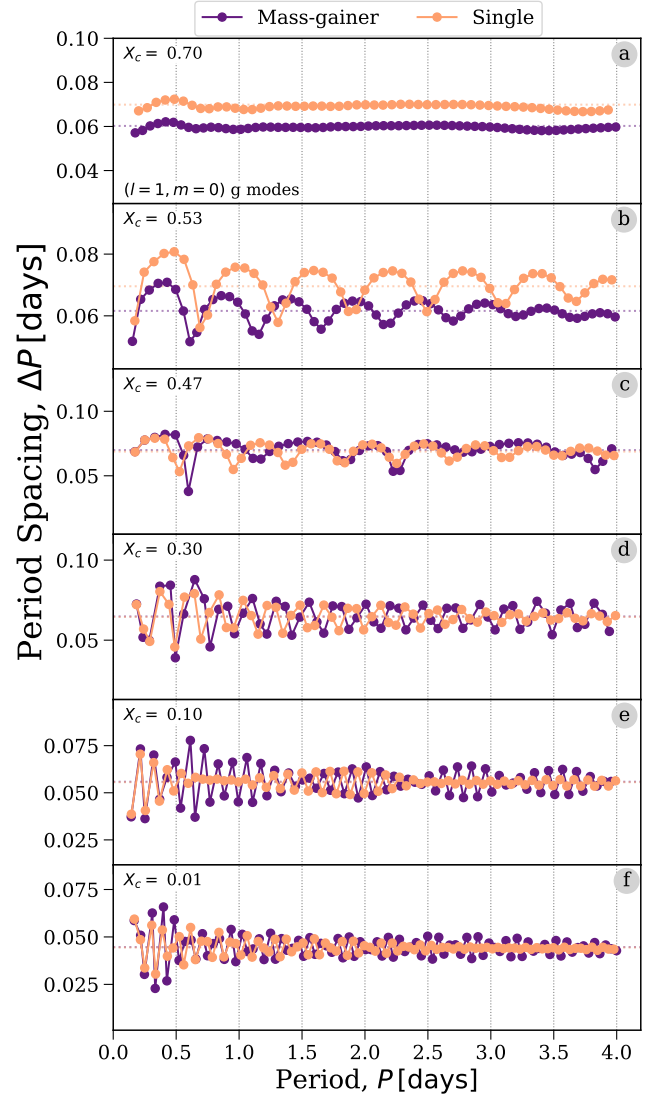


Figure 5. As Figure 2, but showing the period spacing patterns of the $\ell = 1, m = 0$ g -modes. Asymptotic period spacings for each model are shown as dotted lines. We emphasise that the y -axis limits vary by panel.

vective core sizes, resulting in an offset between their asymptotic period spacings.

In subsequent panels (c–f) there are several differences in the period spacing pattern, despite the fact that the stars now have the same mass and convective core size. The two main differences can be expressed in terms of amplitude and phase of oscillations in the period spacing pattern. Frequently in the stars’ later evolution, we note that the amplitude of deviations from the asymptotic spacing are larger for the mass-gainer. This is because the mass-gainer contains regions with steeper chemical composition gradients, which more strongly impact the

Brunt–Väisälä frequency and thus the period of oscillations.

In addition, we find that the period spacing pattern shifts phase in certain regions for the mass gainer. This is most apparent in panel e, in which the patterns are out of phase for periods between ~ 1.5 – 3.2 days and in-phase otherwise. These period-dependent shifts arise due to difference between the Brunt–Väisälä frequency profiles occurring in the region of changing chemical composition. Modes that are sensitive to this region are shifted and so move out of phase, whilst other modes are insensitive to the differences from a single star and thus oscillate with the same periods.

4. DISCUSSION

We have demonstrated that, compared to an equivalent single star, a mass-gainer shows significant differences in its period spacing pattern as a result of accretion altering its chemical composition gradient. In this Section we examine the implications of this result, considering both the impact on current inference modelling, as well as the potential for constraining mass transfer physics.

4.1. Future work

This report summarises the current state of the project after the end of the Kavli Summer Program 2023, however there are still areas that we wish to investigate before submitting the work to a journal.

4.1.1. Implications for inferring stellar properties

Current work considers only single star evolution when inferring stellar properties from period spacing patterns. We have shown that these patterns are significantly changed as a result of mass transfer. Therefore, given that around 20% SPB stars are expected to be in interacted binaries, current methodology may result in incorrect inferences.

We will test how incorrect these inferences may be by fitting the period spacing pattern of our mass-gainer model assuming single star evolution. We will use **GYRE** to compute the periods of $\ell = 1, m = 0$ g -modes for our grid of single star models between 3 and $6 M_{\odot}$ across the entire main sequence. We will then perform a χ^2 fit for a given mass-gainer period spacing pattern with every single star model, at every timestep.

4.1.2. Constraining mass transfer

We will also investigate the possibility for measurements of the period spacing pattern to be used to constrain aspects of mass transfer. For a star that has independent measurements of mass and age, it may be

possible to use the measured period spacing pattern to (i) test whether the star has experienced mass transfer (ii) constrain mass transfer parameters. The latter will only be possible with more models that vary parameters such as mass transfer efficiency and semiconvection in order to assess the sensitivity of the period spacing pattern to these parameters.

4.1.3. Subsequent analysis in a separate paper

In addition to the areas we discuss above, there are several analyses that would not be contained with this work, but that we will recommend as a follow-up to this project.

Grid of binary models—We demonstrate this effect for a single binary model, however further investigations into many binaries (varying initial mass, rate of mass transfer, age of accretor at the onset of mass transfer and metallicity) are required. Additionally, as noted in Section 4.1.2, a larger grid that varies aspects of mass transfer is necessary to assess the sensitivity of our results to these parameters.

Rotation—Our proof of principle analysis uses only non-rotating models, future work should repeat this analysis for models that account for rotation to see how this could affect our results. This is a realistic comparison to many recent studies which only add the effects of rotation at the stage of calculating pulsation frequencies (e.g. [Michielsen et al. 2021](#)).

Analytic distributions—Given the distinct shape of the Brunt–Väisälä frequency profile in our accretor model, it may benefit from an analysis similar to that of [Miglio et al. \(2008\)](#), in which linear perturbation theory could be used to predict the period spacing pattern analytically based on the expected interior structure.

4.2. Caveats

Rotation—Given this analysis acts as a proof of principle, we have limited the scope of our investigations by neglecting rotation in each model. Yet, in reality, we expect that SPB stars will rotate, and this will impact several aspects of our results. In particular, rotation may enhance mixing in the vicinity of the core and alter the chemical composition gradient, which is the key difference between the mass-gainer and single star models.

Diffusive mixing—We enforce a minimum diffusive mixing both as an attempt to counter the lack of rotational mixing and eliminate any numerical artifacts. Given diffusive mixing directly smooths the chemical composition gradient, the choice of the minimum value has also an impact on our results for the Brunt–Väisälä frequency

and period spacing pattern. However, as we demonstrate in Appendix A, differences between the mass-gainer and single star models are still present for a wide-range of choices for this parameter.

Mass-gainer model—The mass-gainer model that we use is formed from a binary in which we artificially ended mass transfer once $0.5 M_{\odot}$ of material was accreted. Although this choice is well motivated, since an accretor with rotation would quickly reach critical rotation and prevent further accretion, the choice may impact our results. Additionally, we only consider a single mass-gainer model for this proof of principle analysis and, though we expect the differences we find will be prevalent across a range of masses and periods, further work is necessary to confirm this.

1 We thank the Kavli Foundation and the Max Planck
 2 Institute for Astrophysics for supporting the 2023 Kavli
 3 Summer Program during which much of this work was
 4 completed. In particular, TW thanks Isabel Thapa,
 5 Stephen Justham and Selma de Mink for their incredible
 6 efforts in organising this program. TW also thanks
 7 Ruggero Valli for his help, and patience, with setting up
 8 MESA on the MPA cluster and sharing the secret com-
 9 mands of `kinit` and `aklog`.

Software: MESA: The MESA EOS is a blend of the OPAL (Rogers & Nayfonov 2002), SCVH (Saumon et al. 1995), FreeEOS (Irwin 2004), HELM (Timmes & Swesty 2000), PC (Potekhin & Chabrier 2010), and Skye (Jermyn et al. 2021) EOSes. Radiative opacities are primarily from OPAL (Iglesias & Rogers 1993, 1996), with low-temperature data from Ferguson et al. (2005) and the high-temperature, Compton-scattering dominated regime by Poutanen (2017). Electron conduction opacities are from Cassisi et al. (2007) and Blouin et al. (2020). Nuclear reaction rates are from JINA REACLIB (Cyburt et al. 2010), NACRE (Angulo et al. 1999) and additional tabulated weak reaction rates Fuller et al. (1985); Oda et al. (1994); Langanke & Martínez-Pinedo (2000). Screening is included via the prescription of Chugunov et al. (2007). Thermal neutrino loss rates are from Itoh et al. (1996). Roche lobe radii in binary systems are computed using the fit of Eggleton (1983). Mass transfer rates in Roche lobe overflowing binary systems are determined following the prescription of Ritter (1988). GYRE (Townsend & Teitler 2013; Townsend et al. 2018), Astropy (Astropy Collaboration et al. 2013, 2018, 2022), Python (Van Rossum & Drake 2009), numpy (Harris et al. 2020), pandas (pandas development team 2022; Wes McKinney 2010), matplotlib (Hunter 2007), scipy (Virtanen et al. 2020)

REFERENCES

Aerts, C., Christensen-Dalsgaard, J., & Kurtz, D. W. 2010, *Asteroseismology* (Springerslowly pulsating B stars), doi: [10.1007/978-1-4020-5803-5](https://doi.org/10.1007/978-1-4020-5803-5)

Aerts, C., Mathis, S., & Rogers, T. M. 2019, *ARA&A*, 57, 35, doi: [10.1146/annurev-astro-091918-104359](https://doi.org/10.1146/annurev-astro-091918-104359)

Almeida, L. A., Sana, H., Taylor, W., et al. 2017, *A&A*, 598, A84, doi: [10.1051/0004-6361/201629844](https://doi.org/10.1051/0004-6361/201629844)

Angulo, C., Arnould, M., Rayet, M., et al. 1999, *NuPhA*, 656, 3, doi: [10.1016/S0375-9474\(99\)00030-5](https://doi.org/10.1016/S0375-9474(99)00030-5)

Astropy Collaboration, Robitaille, T. P., Tollerud, E. J., et al. 2013, *A&A*, 558, A33, doi: [10.1051/0004-6361/201322068](https://doi.org/10.1051/0004-6361/201322068)

Astropy Collaboration, Price-Whelan, A. M., Sipőcz, B. M., et al. 2018, *AJ*, 156, 123, doi: [10.3847/1538-3881/aabc4f](https://doi.org/10.3847/1538-3881/aabc4f)

Astropy Collaboration, Price-Whelan, A. M., Lim, P. L., et al. 2022, *apj*, 935, 167, doi: [10.3847/1538-4357/ac7c74](https://doi.org/10.3847/1538-4357/ac7c74)

Blouin, S., Shaffer, N. R., Saumon, D., & Starrett, C. E. 2020, *ApJ*, 899, 46, doi: [10.3847/1538-4357/ab9e75](https://doi.org/10.3847/1538-4357/ab9e75)

Broekgaarden, F. S., Berger, E., Stevenson, S., et al. 2022, *MNRAS*, 516, 5737, doi: [10.1093/mnras/stac1677](https://doi.org/10.1093/mnras/stac1677)

Brunt, D. 1927, *Quarterly Journal of the Royal Meteorological Society*, 53, 30, doi: [10.1002/qj.49705322103](https://doi.org/10.1002/qj.49705322103)

Cassisi, S., Potekhin, A. Y., Pietrinferni, A., Catelan, M., & Salaris, M. 2007, *ApJ*, 661, 1094, doi: [10.1086/516819](https://doi.org/10.1086/516819)

Christensen-Dalsgaard, J. 2008, *Ap&SS*, 316, 113, doi: [10.1007/s10509-007-9689-z](https://doi.org/10.1007/s10509-007-9689-z)

Chugunov, A. I., Dewitt, H. E., & Yakovlev, D. G. 2007, *PhRvD*, 76, 025028, doi: [10.1103/PhysRevD.76.025028](https://doi.org/10.1103/PhysRevD.76.025028)

Claret, A., & Torres, G. 2017, *ApJ*, 849, 18, doi: [10.3847/1538-4357/aa8770](https://doi.org/10.3847/1538-4357/aa8770)

Cox, A. N., Morgan, S. M., Rogers, F. J., & Iglesias, C. A. 1992, *ApJ*, 393, 272, doi: [10.1086/171504](https://doi.org/10.1086/171504)

Crowe, R. A., & Matalas, R. 1982, *A&A*, 108, 55

Cyburt, R. H., Amthor, A. M., Ferguson, R., et al. 2010, *ApJS*, 189, 240, doi: [10.1088/0067-0049/189/1/240](https://doi.org/10.1088/0067-0049/189/1/240)

Dziembowski, W. A. 1971, *AcA*, 21, 289

Eggleton, P. P. 1983, *ApJ*, 268, 368, doi: [10.1086/160960](https://doi.org/10.1086/160960)

Ferguson, J. W., Alexander, D. R., Allard, F., et al. 2005, *ApJ*, 623, 585, doi: [10.1086/428642](https://doi.org/10.1086/428642)

Fuller, G. M., Fowler, W. A., & Newman, M. J. 1985, *ApJ*, 293, 1, doi: [10.1086/163208](https://doi.org/10.1086/163208)

- Goldstein, J., & Townsend, R. H. D. 2020, *ApJ*, 899, 116, doi: [10.3847/1538-4357/aba748](https://doi.org/10.3847/1538-4357/aba748)
- Harris, C. R., Millman, K. J., van der Walt, S. J., et al. 2020, *Nature*, 585, 357, doi: [10.1038/s41586-020-2649-2](https://doi.org/10.1038/s41586-020-2649-2)
- Herwig, F. 2000, *A&A*, 360, 952, doi: [10.48550/arXiv.astro-ph/0007139](https://doi.org/10.48550/arXiv.astro-ph/0007139)
- Hunter, J. D. 2007, *Computing in Science & Engineering*, 9, 90, doi: [10.1109/MCSE.2007.55](https://doi.org/10.1109/MCSE.2007.55)
- Iglesias, C. A., & Rogers, F. J. 1993, *ApJ*, 412, 752, doi: [10.1086/172958](https://doi.org/10.1086/172958)
- . 1996, *ApJ*, 464, 943, doi: [10.1086/177381](https://doi.org/10.1086/177381)
- Irwin, A. W. 2004, *The FreeEOS Code for Calculating the Equation of State for Stellar Interiors*. <http://freeeos.sourceforge.net/>
- Itoh, N., Hayashi, H., Nishikawa, A., & Kohyama, Y. 1996, *ApJS*, 102, 411, doi: [10.1086/192264](https://doi.org/10.1086/192264)
- Jermyn, A. S., Schwab, J., Bauer, E., Timmes, F. X., & Potekhin, A. Y. 2021, *ApJ*, 913, 72, doi: [10.3847/1538-4357/abf48e](https://doi.org/10.3847/1538-4357/abf48e)
- Jermyn, A. S., Bauer, E. B., Schwab, J., et al. 2023, *ApJS*, 265, 15, doi: [10.3847/1538-4365/aca8d](https://doi.org/10.3847/1538-4365/aca8d)
- Johnston, C. 2021, *A&A*, 655, A29, doi: [10.1051/0004-6361/202141080](https://doi.org/10.1051/0004-6361/202141080)
- Kippenhahn, R., Ruschenplatt, G., & Thomas, H. C. 1980, *A&A*, 91, 175
- Kolb, U., & Ritter, H. 1990, *A&A*, 236, 385
- Kurtz, D. W. 2022, *ARA&A*, 60, 31, doi: [10.1146/annurev-astro-052920-094232](https://doi.org/10.1146/annurev-astro-052920-094232)
- Langanke, K., & Martínez-Pinedo, G. 2000, *Nuclear Physics A*, 673, 481, doi: [10.1016/S0375-9474\(00\)00131-7](https://doi.org/10.1016/S0375-9474(00)00131-7)
- Langer, N., Fricke, K. J., & Sugimoto, D. 1983, *A&A*, 126, 207
- Ledoux, P. 1947, *ApJ*, 105, 305, doi: [10.1086/144905](https://doi.org/10.1086/144905)
- Mason, B. D., Hartkopf, W. I., Gies, D. R., Henry, T. J., & Helsel, J. W. 2009, *AJ*, 137, 3358, doi: [10.1088/0004-6256/137/2/3358](https://doi.org/10.1088/0004-6256/137/2/3358)
- Michielsen, M., Aerts, C., & Bowman, D. M. 2021, *A&A*, 650, A175, doi: [10.1051/0004-6361/202039926](https://doi.org/10.1051/0004-6361/202039926)
- Miglio, A., Montalbán, J., Eggenberger, P., & Noels, A. 2008, *Astronomische Nachrichten*, 329, 529, doi: [10.1002/asna.200710991](https://doi.org/10.1002/asna.200710991)
- Miszuda, A., Szewczuk, W., & Daszyńska-Daszkiewicz, J. 2021, *MNRAS*, 505, 3206, doi: [10.1093/mnras/stab1597](https://doi.org/10.1093/mnras/stab1597)
- Mitalas, R. 1972, *ApJ*, 177, 693, doi: [10.1086/151748](https://doi.org/10.1086/151748)
- Moe, M., & Di Stefano, R. 2017, *ApJS*, 230, 15, doi: [10.3847/1538-4365/aa6fb6](https://doi.org/10.3847/1538-4365/aa6fb6)
- Neo, S., Miyaji, S., Nomoto, K., & Sugimoto, D. 1977, *PASJ*, 29, 249
- Oda, T., Hino, M., Muto, K., Takahara, M., & Sato, K. 1994, *Atomic Data and Nuclear Data Tables*, 56, 231, doi: [10.1006/adnd.1994.1007](https://doi.org/10.1006/adnd.1994.1007)
- Packet, W. 1981, *A&A*, 102, 17
- Pamyatnykh, A. A. 1999, *AcA*, 49, 119
- pandas development team, T. 2022, *pandas-dev/pandas: Pandas 1.4.2, v1.4.2*, Zenodo, doi: [10.5281/zenodo.6408044](https://doi.org/10.5281/zenodo.6408044)
- Paxton, B. 2023, *Modules for Experiments in Stellar Astrophysics (MESA), r23.05.1*, Zenodo, doi: [10.5281/zenodo.7983526](https://doi.org/10.5281/zenodo.7983526)
- Paxton, B., Bildsten, L., Dotter, A., et al. 2011, *ApJS*, 192, 3, doi: [10.1088/0067-0049/192/1/3](https://doi.org/10.1088/0067-0049/192/1/3)
- Paxton, B., Cantiello, M., Arras, P., et al. 2013, *ApJS*, 208, 4, doi: [10.1088/0067-0049/208/1/4](https://doi.org/10.1088/0067-0049/208/1/4)
- Paxton, B., Marchant, P., Schwab, J., et al. 2015, *ApJS*, 220, 15, doi: [10.1088/0067-0049/220/1/15](https://doi.org/10.1088/0067-0049/220/1/15)
- Paxton, B., Schwab, J., Bauer, E. B., et al. 2018, *ApJS*, 234, 34, doi: [10.3847/1538-4365/aaa5a8](https://doi.org/10.3847/1538-4365/aaa5a8)
- Paxton, B., Smolec, R., Schwab, J., et al. 2019, *ApJS*, 243, 10, doi: [10.3847/1538-4365/ab2241](https://doi.org/10.3847/1538-4365/ab2241)
- Pedersen, M. G. 2022, *ApJ*, 930, 94, doi: [10.3847/1538-4357/ac5b05](https://doi.org/10.3847/1538-4357/ac5b05)
- Pedersen, M. G., Aerts, C., Pápics, P. I., & Rogers, T. M. 2018, *A&A*, 614, A128, doi: [10.1051/0004-6361/201732317](https://doi.org/10.1051/0004-6361/201732317)
- Potekhin, A. Y., & Chabrier, G. 2010, *Contributions to Plasma Physics*, 50, 82, doi: [10.1002/ctpp.201010017](https://doi.org/10.1002/ctpp.201010017)
- Poutanen, J. 2017, *ApJ*, 835, 119, doi: [10.3847/1538-4357/835/2/119](https://doi.org/10.3847/1538-4357/835/2/119)
- Renzo, M., & Götberg, Y. 2021, *ApJ*, 923, 277, doi: [10.3847/1538-4357/ac29c5](https://doi.org/10.3847/1538-4357/ac29c5)
- Ritter, H. 1988, *A&A*, 202, 93
- Rogers, F. J., & Nayfonov, A. 2002, *ApJ*, 576, 1064, doi: [10.1086/341894](https://doi.org/10.1086/341894)
- Sana, H., de Mink, S. E., de Koter, A., et al. 2012, *Science*, 337, 444, doi: [10.1126/science.1223344](https://doi.org/10.1126/science.1223344)
- Saumon, D., Chabrier, G., & van Horn, H. M. 1995, *ApJS*, 99, 713, doi: [10.1086/192204](https://doi.org/10.1086/192204)
- Silva Aguirre, V., Ballot, J., Serenelli, A. M., & Weiss, A. 2011, *A&A*, 529, A63, doi: [10.1051/0004-6361/201015847](https://doi.org/10.1051/0004-6361/201015847)
- Sun, M., Townsend, R. H. D., & Guo, Z. 2023, *ApJ*, 945, 43, doi: [10.3847/1538-4357/acb33a](https://doi.org/10.3847/1538-4357/acb33a)
- Tassoul, M. 1980, *ApJS*, 43, 469, doi: [10.1086/190678](https://doi.org/10.1086/190678)
- Timmes, F. X., & Swesty, F. D. 2000, *ApJS*, 126, 501, doi: [10.1086/313304](https://doi.org/10.1086/313304)
- Townsend, R. H. D., Goldstein, J., & Zweibel, E. G. 2018, *MNRAS*, 475, 879, doi: [10.1093/mnras/stx3142](https://doi.org/10.1093/mnras/stx3142)
- Townsend, R. H. D., & Teitler, S. A. 2013, *MNRAS*, 435, 3406, doi: [10.1093/mnras/stt1533](https://doi.org/10.1093/mnras/stt1533)

- Van Rossum, G., & Drake, F. L. 2009, Python 3 Reference Manual (Scotts Valley, CA: CreateSpace)
- Virtanen, P., Gommers, R., Oliphant, T. E., et al. 2020, Nature Methods, 17, 261, doi: [10.1038/s41592-019-0686-2](https://doi.org/10.1038/s41592-019-0686-2)
- Väisälä, V. 1925, Soc. Sci. Fennica, Commentationes Phys.-Math. II, 19, 38.
<https://cir.nii.ac.jp/crid/1571417125137427072>
- Waelkens, C. 1991, A&A, 246, 453
- Waelkens, C., & Rufener, F. 1985, A&A, 152, 6
- Wes McKinney. 2010, in Proceedings of the 9th Python in Science Conference, ed. Stéfan van der Walt & Jarrod Millman, 56 – 61, doi: [10.25080/Majora-92bf1922-00a](https://doi.org/10.25080/Majora-92bf1922-00a)

APPENDIX

A. IMPORTANCE OF CHOICE OF MINIMUM DIFFUSIVE MIXING

In our MESA models we set a minimum diffusive mixing coefficient, D_{\min} , in order to account for mixing processes not included in our model and to mix over unphysical numerical composition gradients. For our models analysed in this paper we set $D_{\min} = 20 \text{ cm}^2 \text{ s}^{-1}$, in this Appendix we explore the impact that this choice has on our results.

We repeated our binary MESA simulations for four additional choices of D_{\min} , ranging from $1 - 100 \text{ cm}^2 \text{ s}^{-1}$. In Figure A1 we compare the Brunt–Väisälä frequency profiles of these models at a central hydrogen abundance of $X_c = 0.1$, where the lower panel zooms in on the highlighted region in the upper panel. There are significant differences in the profiles between the different models. As one may expect, lower mixing coefficients lead to steeper composition gradients and therefore sharper features in the Brunt–Väisälä frequency and stronger signals in the period spacing pattern.

However, an overly low choice of D_{\min} leads to numerical glitches in the composition gradient and the Brunt–Väisälä frequency profile. We highlight this in Figure A1, where glitches are clearly visible in both the $D_{\min} = 1 \text{ cm}^2 \text{ s}^{-1}$ and $D_{\min} = 10 \text{ cm}^2 \text{ s}^{-1}$ models.

We explored a more dense grid of D_{\min} models and found that $D_{\min} = 20 \text{ cm}^2 \text{ s}^{-1}$ was the smallest level of mixing that still removed numerical glitches, which in-

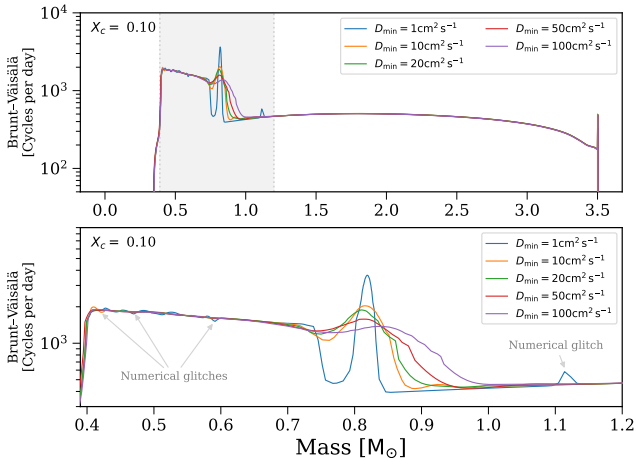


Figure A1. Comparison of the impact of changing the MESA minimum diffusive mixing parameter, D_{\min} , on the Brunt–Väisälä frequency profile. Bottom panel zooms in on the highlighted range in the top panel. Annotations highlight numerical glitches in low D_{\min} models.

formed our selection of this model as the default choice in this paper. This level of mixing is not unexpected, since mass transfer will likely induce rotation in the accretor (Packet 1981) and this leads to rotational mixing.

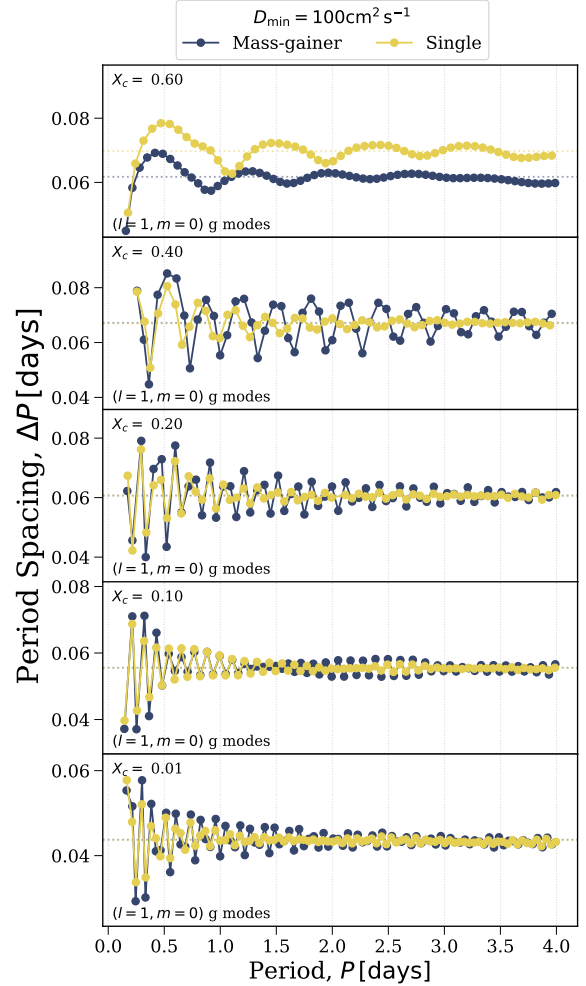


Figure A2. As Figure 5, but with the minimum diffusive mixing coefficient set to $D_{\min} = 20 \text{ cm}^2 \text{ s}^{-1}$.

We stress that the qualitative differences between the mass-gainer and single star in the period spacing patterns remain the same for all choices of D_{\min} that we explored. To highlight this point we show the period spacing pattern for the model with $D_{\min} = 100 \text{ cm}^2 \text{ s}^{-1}$ in Figure A2. Despite slight differences to the exact shape of the pattern, we still find the same features of (i) stronger ΔP for mass-gainers and (ii) regions in which the period spacing is in-phase and regions in which it is out of phase between the mass-gainer and single star.